Separation and Unsteady Vortex Shedding from Leading Edge Surface Roughness

B.D. Matheis
Iowa State University
2271 Howe Hall, Room 1200
Ames, IA 50011-2271

Email: bmatheis@iastate.edu

W.W. Huebsch
West Virginia University
P.O. Box 6106, Room 333 ESB
Morgantown, WV 26506-6106

Email: wade.huebsch@mail.wvu.edu

A.P. Rothmayer
Iowa State University
2271 Howe Hall, Room 1200
Ames, IA 50011-2271

Email: roth@iastate.edu

ABSTRACT

The properties of isolated and distributed surface roughness, as well as their effects on transition, separation and overall airfoil performance, are reviewed for steady and unsteady flows. Ongoing research aimed at developing Direct Numerical Simulation tools for the study of leading edge roughness is discussed, and representative calculations are presented for steady and unsteady flows past two and three-dimensional isolated and distributed roughness on airfoil leading edges. Preliminary two-dimensional computations of the suppression of flow separation using dynamic surface roughness are also presented.

1.0 LEADING EDGE ROUGHNESS AND AIRCRAFT PERFORMANCE

The lift and drag performance of an aerodynamic surface, such as an airfoil or a wing, is highly dependent on the state of the boundary layer. The performance specifications of such surfaces typically assume that the wing is smooth and has no imperfections. However, when the wing becomes exposed to the environment, dirt, insect debris, frost formation and other imperfections can lead to the presence of small roughness on the surface, Brumby (1979). The impact on the performance of the wing has been documented by a number of authors, cf. Hood (1939), Ljungstromm (1972), Brumby (1979), Bragg & Gregorek (1989), Oolbekkink & Volkers (1991), Boer & Van Hengst (1993), Valarezo *et al.* (1993) and Tezok *et al.* (1998). These experimental studies typically place sand-paper on the airfoil surface in order to simulate the presence of

Paper presented at the RTO AVT Specialists' Meeting on "Enhancement of NATO Military Flight Vehicle Performance by Management of Interacting Boundary Layer Transition and Separation", held in Prague, Czech Republic, 4-7 October 2004, and published in RTO-MP-AVT-111.

roughness. All roughness studies have shown that the largest performance decrement is due to roughness which is located within about 5% chord of the leading edge. Covering the rest of the surface with roughness results in only a relatively small additional degradation in performance. Because of this, and the fact that most surface roughness occurs near the leading edge, the study of surface roughness on the front portion of an airfoil and its impact on performance has received considerable attention.

The three major effects of roughness on airfoil performance are: a decrease in the lift at a given angle-of-attack, a reduction of the stall angle-of-attack, and an increase in the parasite drag, Valarezo *et al.* (1993). The reduction in maximum lift coefficient and stall angle-of-attack is typically 20-35%, Ljungstromm (1972), Boer & Van Hengst (1993), Valarezo *et al.* (1993) and Tezok *et al.* (1998), depending on the roughness geometric factors and freestream conditions. The increase in parasite drag due to leading edge roughness is typically about 15%, Tezok *et al.* (1998).

For all aircraft types, an increase in the parasite drag means an increase in the fuel burned and a resulting decrease in the operational range of the aircraft. For fighter aircraft, in particular, the effect of leading edge roughness could be even more critical, since the performance margins are typically smaller and maintaining the design performance levels could mean the difference between success or failure of the mission. Additionally, it is well known among the aircraft icing community that aerodynamic surfaces with a small leading edge radius of curvature are the best collectors of freestream water droplets. It can be expected that fighter aircraft, with their "sharper" leading edges will have a greater tendency to accumulate roughness due to dirt and insects in the freestream. Figure 1, taken from Braslow *et al*. (1966), shows the zero-lift drag of several aircraft types, including a fighter aircraft, when leading edge roughness is present.

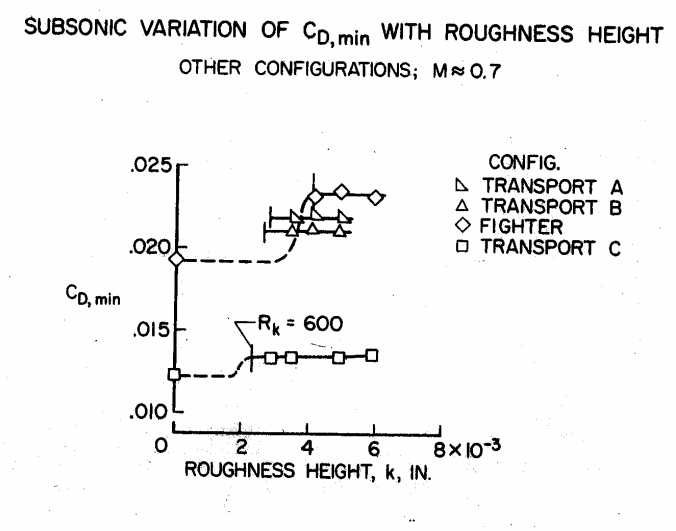

Figure 1. Increase in the zero-lift drag due to surface roughness for various types of aircraft, from Braslow *et al.* (1966)

The roughness used in the Braslow *et al*. (1966) experiments is of the sand-paper type placed in the leading edge region. In Figure 1, k is the maximum roughness height, so that k=0 is the clean airfoil. The figure shows the zero-lift drag as a function of this roughness height. Another important parameter used to assess the impact of roughness is the roughness Reynolds number, Re_k (R_k in Figure 1), given by

$$Re_k = \frac{ku_k}{\nu} \quad (1)$$

where u_k is the velocity at the height of the roughness without the roughness present and ν is the kinematic viscosity. Figure 1 shows that as the roughness height is increased from zero there is initially little impact of the roughness on the zero-lift drag. A sudden increase in the drag occurs when the value of Re_k reaches the critical value of 600, shown by the vertical tick marks on each curve in Figure 1. This is the value of Re_k at which Braslow *et al*. (1966) first observed a premature roughness induced transition to turbulence with the transition region essentially beginning at the roughness location.

While natural roughness tends to degrade the performance of an aerodynamic surface, it is possible to use synthetic roughness as a means to improve performance under certain conditions. One example of this is the suppression of a leading edge separation bubble. A leading edge separation bubble tends to reduce the lift of the airfoil and potentially leads to a premature clean airfoil transition, Tani (1969). Various flow control methods have been investigated for suppressing this separation bubble, one of them being *dynamic roughness*. The authors define dynamic roughness (Huebsch, 2004) as small time-dependent perturbations to the airfoil or wing surface as a potential mechanism for controlling the flow separation. In the most basic form, roughness elements are placed in the leading-edge region of the wing that would have the ability to expand and contract at a specific frequency and amplitude such that flow separation is delayed or eliminated for a certain flight condition.

2.0 SEPARATION, VORTEX SHEDDING AND ROUGHNESS INDUCED TRANSITION

The desire to limit the negative impact of surface roughness on airfoil performance has led to a great deal of study into the mechanisms whereby roughness promotes early transition. The roughness geometry which is usually of interest, and most applicable to aircraft performance, is a distributed field of three-dimensional roughness on the leading edge. When the roughness field is sparse enough, the flow behaves like that over isolated three-dimensional roughness elements, Kendall (1990). Additionally, when the roughness field has a relatively short chordwise extent and is densely packed then the transition process is similar to transition due to a two-dimensional trip, Braslow *et al.* (1966). In the next few sections we review previous studies which have examined the mechanisms whereby these different types of roughness cause premature transition. The focus of this review is the role played by separation and vortex structures generated by the roughness in promoting transition. Additionally, we review previous work which has sought to use dynamic surface roughness to eliminate leading edge separation and vortex structures. Before we discuss transition due to surface roughness we review the process by which the flow transitions to turbulence on a clean airfoil, again with emphasis on the role played by the vortex structures.

2.1 Properties of clean airfoil transition

The process of transition on a clean airfoil in low disturbance environments is relatively well understood and is qualitatively similar to transition on a flat plate. Once freestream disturbances are ingested by the boundary layer through a receptivity mechanism they undergo exponential growth in a region governed by linearized equations. For airfoils this is the growth of Tollmien-Schlichting (T-S) waves while for swept wings the dominant instability is the cross-flow mode, Saric *et al.* (2003). In either case, once the disturbance amplitudes have grown sufficiently, a secondary instability arises which eventually leads to non-linear growth and produces streamwise vortices, Tani (1969). The streamwise vortices play an important role in the

remaining transition process as they work to redistribute the streamwise momentum vertically and lift spanwise vorticity from the surface, resulting in the "high shear layer", Tani (1969). This "high shear layer" generates hairpin vortices which break down into smaller vortices as they convect downstream, ultimately leading to the formation of turbulent spots. The turbulent spots then grow and merge to form a fully turbulent boundary layer. The transition region on an airfoil is longer than the transition region on a flat plate due to the favourable pressure gradient on the forward portion of the airfoil.

The presence of roughness on the surface can alter the transition process in a number of ways. For example, roughness can enhance the instability of the T-S modes or introduce new unstable modes. Roughness can also enhance the receptivity of the boundary layer, or bypass linear instability mechanisms altogether by acting as a source of additional disturbances, such as through the vortex shedding process, Bushnell (1989) and Fasel *et al*. (1977). The term bypass transition was coined by Morkovin (1969) to encompass those transition processes which are not initiated via the traditional T-S instability. The vortex structures generated by three-dimensional roughness are similar to the vortex structures which are seen in various stages of the clean airfoil transition process described above. For example, three-dimensional roughness generates streamwise counter-rotating vortices, Gregory & Walker (1956), similar to those which generate the "high shear layer" in the clean airfoil transition. Additionally, when a certain value of Re_k is reached, hairpin vortices are shed from three-dimensional roughness, and these ultimately break down and lead to turbulent spots, causing a rapid forward movement of the transition point. This process "bears resemblance to the final instability in the transitions commencing with T-S waves as the primary instability", Morkovin (1984).

2.2 Separation from two-dimensional roughness

The mechanism by which two-dimensional roughness enhances transition was studied extensively by Klebanoff & Tidstrom (1972). The characteristic feature of flow over two-dimensional roughness is a long separation bubble which extends 40-50k downstream of the roughness, Morkovin (1990). The velocity profiles within this recovery region are highly inflectional which leads to a type of inviscid instability known as a Rayleigh instability, Schlichting (2000). The amplification rates for this type of instability are much higher than in the Blasius flow and the onset of the secondary instabilities occurs much sooner. The study by Klebanoff & Tidstrom (1972) confirms that premature transition due to two-dimensional roughness is caused by large amplification of T-S waves in the separation region behind the roughness. Other studies by Cebecci & Egan (1989) and Masad & Iyer (1994) have also shown the destabilizing effect of the separation region. Since the transition is directly tied to the separation region, longer separations will generally mean larger total amplification of the T-S waves. For this reason we use Navier-Stokes simulations to examine the separation region behind two-dimensional roughness elements on an airfoil leading edge and assess the impact of varying roughness size and location as well as the freestream Reynolds number, see Section 3.1, Figure 2 and Figure 4a.

2.3 Separation and vortex shedding from isolated three-dimensional roughness

The separation region behind isolated three-dimensional roughness is significantly shorter, about 3-6k, and amplification of T-S waves is not significant, Morkovin (1990). As Re_k increases, a pair of chimney vortices form in the wake which rise normal to the surface and are then turned downstream, creating a pair of counter-rotating streamwise vortices, Gregory & Walker (1956). Additionally, horse-shoe vortices may form upstream with the legs extending into the roughness wake, forming a second pair of streamwise vortices closer to the surface. At some value $Re_{k,shed}$ hairpin vortices begin to be shed periodically into the wake. For a hemispherical roughness on a flat plate this shedding begins at an Re_k of about 400. Initially, the hairpin vortices convect out of the boundary layer without breaking down into secondary structures, Norman (1972).

Eventually an Re_k is reached (about 550 for roughness on a flat plate) where the vortices do break down, "probably as an interaction of the horseshoe vortex and the inter-twined legs of the hairpin vortices", Morkovin (1984,1990). Initially the beginning of the transition region is located 3-5k downstream of the roughness. However as Re_k increases to the critical value $Re_{k,crit}$ (about 600 for roughness on a flat plate) the transition region rapidly approaches the roughness location.

The process of hairpin vortex shedding and break-down was experimentally examined by Acarlar & Smith (1987). In general, they observed hairpin vortex formation in the region 0-3k downstream of the roughness with vortex growth and evolution occurring 3-15k downstream of the roughness. The evolution consists of a lift-up of the vortex head due to self induction effects while the vortex legs weakened in vorticity and began to stretch parallel to the wall. One of the significant secondary structures observed is a secondary vortex head on the roughness center-plane which is generated by a shear layer created by the original hairpin vortex legs. Recall that the hairpin vortices in the clean airfoil transition are generated from a "high shear layer".

Isolated three-dimensional roughness on an airfoil leading edge has been studied experimentally by Gregory & Walker (1956), Peterson & Horton (1959), Bragg *et al.* (1995,1996), and Cummings & Bragg (1996). One of the most significant differences in comparison with roughness on a flat plate is an increase in the roughness Reynolds number at which the various events take place. For example, Bragg *et al.* (1995) measured $Re_{k,crit}$ values as high as 1500 on a NACA 0012 airfoil leading edge. Additionally, this work showed that the roughness induced transition on a leading edge requires a considerable streamwise extent to develop into a fully turbulent boundary layer. It should be noted that some researchers, such as Peterson & Horton (1959) have found values of $Re_{k,crit}$ near 600 in a strongly favourable pressure gradient. However, their criterion is based on the first observation of non-zero u_{rms} values, as opposed to the rapid approach of the transition location to the roughness element as first used by Tani (1961) and Tani *et al.* (1962). Another significant difference for isolated roughness on a leading edge is that the approach of the transition region to the roughness location at $Re_{k,crit}$ is more rapid than for a flat plate, Gregory & Walker (1956).

2.4 Separation and vortex shedding from distributed roughness

As opposed to isolated roughness, a good deal of distributed roughness research has been conducted in favourable pressure gradients, i.e. on the leading edge. Unfortunately the process of transition due to distributed roughness is not nearly as well understood as the isolated case. Morkovin (1990) suggests a few possibilities, including an increased receptivity, amalgamation of streamwise vorticity leading to a new linear instability, and an increase in the disturbance level via direct eddy shedding, among others.

Experimental evidence by Leventhal (1981), Tadjfar *et al*. (1985) and Corke *et al.* (1986) indicate that transition induced by distributed roughness is not simply due to an amplification of T-S waves. These findings are confirmed in analytical studies by Singh & Lumley (1971) and Aldoss (1982). The DNS study by Floryan *et al*. (1992) does show that transition due to distributed roughness is dominated by a linear instability mechanism which is not the T-S mechanism.

In terms of a critical roughness Reynolds number, Braslow *et al*. (1966) show that distributed roughness behaves similarly to isolated three-dimensional roughness. Near the leading edge there is an increase in the value of $Re_{k,crit}$, which they identify as an Re_x effect. Further back from the stagnation point, once the value of Re_x is greater than about 150,000, the value of $Re_{k,crit}$ is approximately constant at a value of 600 (when Re_k is based on the maximum roughness height). Kerho (1995) and Kerho & Bragg (1997) saw a decrease in the value of $Re_{k,crit}$ for their particular roughness distribution placed on an airfoil leading edge. The roughness elements were constant height hemispheres with staggered but constant spacing. Kerho (1995) and Kerho &

Bragg (1997) saw three different types of transition depending on the roughness parameters and freestream conditions. The first was simply an early T-S type transition. The second was linear growth of u_{rms} values just downstream of the roughness followed by an asymptotic approach to a fully turbulent boundary layer. The third type of transition observed by Kerho & Bragg (1997) consists of a short delay with relatively little activity, followed by linear growth of u_{rms} values and again an asymptotic approach to a fully turbulent boundary layer. This third type of transition, which is induced by a roughness field with a short streamwise extent, behaves similarly to a two-dimensional trip which was also tested by Kerho & Bragg (1997). In addition, u_{rms} profiles indicate evidence of hairpin vortex shedding for this particular case.

2.5 Control of flow separation through periodic excitation

Significant progress has been made in flow control for separation and transition. Some examples of past flow control efforts include the use of riblets (Sundaram *et al*., 1996), laminar flow control with boundary layer blowing, suction or wall cooling, and bubble injection and polymer addition for turbulent boundary layers. For flow control on two-dimensional airfoils, a common mechanism has been blowing or suction. Generally, steady blowing is more effective than steady suction. However, both are largely impractical for application to real systems, in that they require a greater power input to effect separation control than the power savings due to any resulting lift enhancement and/or drag reduction. Recently, Greenblatt and Wygnanski (2000) have found that unsteady, periodic excitation can be as much as two orders of magnitude more efficient than steady blowing in the control of steady airfoil separation, for both a leading edge separation bubble and trailing edge flap separation. Periodic excitation of the surface, such as dynamic roughness, could also be used to produce the same separation control effect, both for the steady separation and the dynamic stall cases. Dynamic roughness elements would potentially not require an air plenum and associated plumbing, should have the potential to more easily be applied to three-dimensional problems (e.g., swept wing flows with spanwise instabilities and/or separations), and also potentially would have lower power requirements.

The basic flow control mechanism for periodic blowing (and dynamic roughness) for the two-dimensional geometries is thought to be an injection of vorticity with an increased generation of the large coherent structures in the separated boundary layer or turbulent shear layer, leading to an increase of entrainment, and a transfer of high-momentum fluid toward the wall. This enables the boundary layer to withstand higher adverse pressure gradients than when the excitation is absent. For turbulent shear layers, it is likely that optimum excitation frequencies exist to match the most unstable wavelengths and frequencies of the time mean velocity profiles.

With respect to time-dependent surface perturbations, work has been done for both internal and external flows, such as wall oscillations (e.g. Lekoudis & Sengupta, 1986) and compliant surfaces (e.g. Bushnell, *et al*., 1977) as a means of flow control and skin friction drag reduction. For external flow applications, the work by Duck (1990) and Duck (1985), in part, investigated external incompressible flow past an unsteady wall distortion through the use of triple-deck theory. Results from this work showed that the disturbances from the unsteady perturbation tend to grow as they move downstream as a result of triggering the T-S instability. Rediniotis *et al*. (2002) have conducted preliminary work in the use of an active “smart” skin for turbulent drag reduction in aerodynamic flows. The skin is actively deformed to mimic a traveling wave, which is based on evidence that shows transverse traveling waves with specific characteristics can result in turbulent drag reduction. This indicates that the character of the dynamic motion of the roughness may be as important as the placement, frequency, and maximum amplitude in flow control. Folk & Ho (2001) used MEMS devices to activate micro bubbles on the surface of a delta wing. The surface perturbations alter the global vortex pair and are being used as a method of maneuvering the aircraft. It is pointed out that small-scale perturbations are able to create large global changes in the vortex system due to the fact that flow separation is extremely sensitive to perturbations at the separation point, or separation line.

Greenblatt & Wygnanski (2000) provide a review of the control of flow separation from aerodynamic surfaces through periodic excitation. Much of the work reviewed focuses on oscillatory blowing to achieve the periodic excitation. There has been a fair amount of successful work in this area that has produced a methodology for control of flow separation and an increase in C_L values for airfoils and wings. Entrainment and momentum exchange are increased due to the resulting increase in the strength and organization of the large coherent structures in the mixing layer. These coherent structures consist of transverse vortices or rolls that convect at the average of the velocities of the two streams, and engulf fluid from one side of the layer and carry it to the other side. One key finding is that the entrainment of the boundary layer can be significantly altered by small amplitude excitation. Whether the mechanism is oscillatory blowing, vibrating ribbons, or piezoelectric-based diaphragms, the result is an oscillatory addition of momentum to the fluid which can impact flow separation. All of the mechanisms provide a perturbation to the near-surface flow, as does surface roughness.

Periodic excitation through oscillatory blowing has been shown to increase C_{lmax} somewhat, but the biggest gains in lift are in the post-stall region. The excitation location must be at or near the naturally occurring separation location in order to be effective. A study of oscillatory blowing on a NACA 0015 airfoil with a 25% chord flap by Seifert, et al. (1993) demonstrated significant increases in C_l and reductions in C_d. These results were insensitive to Reynolds number. Dynamic stall has also been controlled via two-dimensional oscillatory slot blowing (Greenblatt and Wygnanski, 2001a, b). Here, nearly identical or somewhat larger C_l values were obtained, but without hysteresis in lift or the large negative pitching moment excursions that occur without periodic excitation.

White and Saric (2000) examined roughness effects on transition and found that three-dimensional static roughness could be an effective tool in delaying the transition to turbulence on a swept wing. The three-dimensional static roughness was chosen to have a spanwise wavelength that was significantly smaller than the spanwise wavelength of the dominant instability mode for the three-dimensional transition process. Excited disturbances were shorter than the most unstable wavelength; these disturbances grew and then decayed without inducing transition. Transition was delayed from before mid-chord to beyond 80% x/c for this aft-loaded airfoil. They also reported initial tests of a three-dimensional variable roughness (i.e. dynamic roughness) generator consisting of thin polyester tape mounted on the wing surface above an array of 3 mm diameter holes and a pressurized plenum within the wing model. Roughness height could be varied as a function of the plenum pressure. In their initial tests, transition was successfully enhanced by the variable roughness deformation. This was taken as an indication that transition delay was also feasible.

2.6 Summary and the use of Direct Numerical Simulation (DNS)

In summary, previous research indicates that transition due to two-dimensional and isolated three-dimensional surface roughness is directly tied to the separation and vortex structures which are generated by the roughness. However these phenomena have not been extensively studied for roughness which is located on an airfoil leading edge. In addition, the relationship between separation and vortex shedding from distributed roughness and transition due to distributed roughness is not well understood. For these reasons, a DNS approach is being used to examine separation and vortex shedding from roughness on an airfoil leading edge.

Additionally, preliminary two-dimensional results are presented here for the effects of dynamic roughness on aerodynamic flow separation. A primary objective associated with dynamic roughness is the delay or elimination of flow separation from an aerodynamic surface. Other objectives include the delay of boundary layer transition or reducing the skin-friction drag once the boundary layer is fully turbulent.

The DNS method used here is a streamfunction-like/vorticity approach developed by Davis *et al.* (1989) for three-dimensional flows. Details of the numerical method can be found in Huebsch (2000), Huebsch & Rothmayer (2001,2002,2004), Matheis *et al.* (2003) and Matheis & Rothmayer (2004).

3.0 SIMULATION OF ISOLATED ROUGHNESS ELEMENTS

3.1 Two-dimensional Simulations

Several isolated roughness cases were run with the two-dimensional Navier-Stokes algorithm. The first is a single two-dimensional roughness on the upper surface of the leading-edge, with the roughness fully contained within the boundary layer. The roughness height is approximately 1/3 of the approaching laminar boundary layer height. Streamfunction and vorticity contours are shown in Figure 2. This particular case is at a constant angle-of-attack of K = 0.0 (K is the angle-of-attack parameter, see Werle & Davis (1971)), Re_R = 1000 (R=leading edge radius of curvature, see Figure 5). Both the steady and unsteady flow solvers were applied to this case, and produce identical results. The unsteady flow solver converges to a steady solution. As the figure shows, the roughness geometry produces a small steady, laminar separation bubble on the downstream-side of the roughness. Grid independence of the flow solution was periodically checked throughout the course of this work. For a grid independent solution, the required grid resolution is approximately 40 to 50 streamwise grid points per roughness diameter. As expected, the evaluation of grid dependence in this work revealed that increases in roughness complexity and flow gradients require a finer grid to resolve the flow physics correctly.

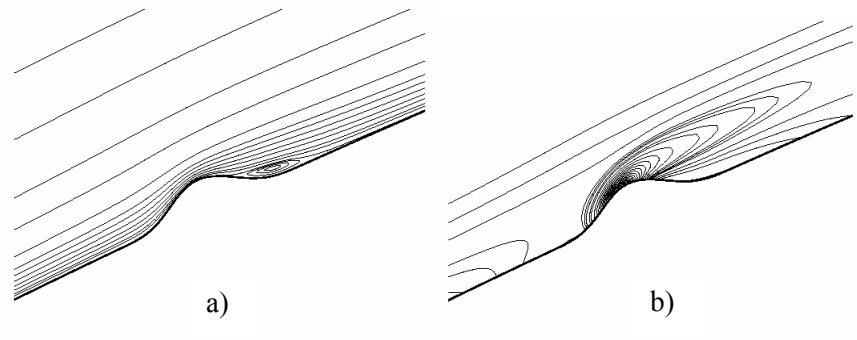

Figure 2. Laminar flow past single leading-edge hump: a) stream function contours and b) vorticity contours.

The other isolated two-dimensional roughness investigation focused on a comparison to the critical roughness Reynolds number ($Re_{k,crit}$). The experimental study by Bragg *et al*. (1995) showed that for an airfoil leading edge with surface roughness, the $Re_{k,crit}$ values are larger than the classic critical value of 600 when the roughness is on a flat plate. In the experiment, isolated three-dimensional hemispheres were placed at various locations downstream of a NACA 0012 leading edge and the chord Reynolds number was varied. For the two-dimensional Navier-Stokes simulations, roughness elements were placed at various chordwise locations which fall within the experimental test range and one experimental hump height was selected, k = 0.5 mm. The roughness matches the basic geometry of the experiment, but is two dimensional. At a given chord location, the free stream Reynolds number was increased to increase the value of Re_k.

Figure 3 summarizes the results of the roughness Reynolds number study. Included in this plot are the experimental results from Bragg *et al*. (1995) for the critical roughness Reynolds number values. Using several leading-edge locations for the isolated roughness and varying the value of Re_k, the results of the simulation show the regimes where the resulting flow is steady and laminar, or unsteady with vortex shedding. At each roughness location, the plot shows the point where the computed flow is steady and laminar. Everywhere below that point the flow is also steady and laminar, as verified by further computations. Likewise, a point is shown at a higher Re_k value where the flow was fully unsteady with vortex shedding. Everywhere above that point the flow remains in this state. This results in the shaded areas of unsteady vortex shedding and steady, laminar flow. As the plot shows, there is not a clear delineation between the two regions. Simulations were performed for cases that fall in between the shaded regions; the results showed no vortex shedding, but did show clear unsteadiness within the separation bubble aft of the roughness. Therefore, the data points indicating "unsteady vortex shedding" (and the shaded region above) on the plot have fully unsteady flow with vortex shedding downstream of the roughness element. The unsteady vortex shedding results are in relatively good agreement with the critical roughness Reynolds number at lower values of Re_k, but diverge as the roughness Reynolds number is increased. This is a possible indication that there is a correlation between the observed unsteady vortex-shedding as calculated by the two-dimensional algorithm and the roughness-induced transitional flow seen in the experiments for this type of large-scale roughness.

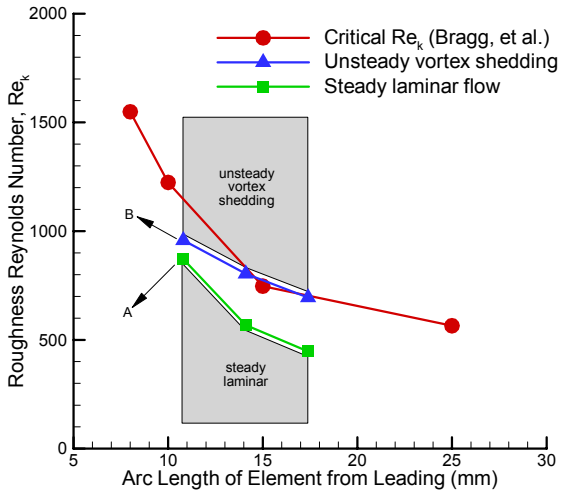

Figure 3. Comparison of steady laminar and unsteady vortex-shedding flow past roughness element to critical roughness Reynolds number.

It is worth noting the differences between the experiment and the computations in the determination of the roughness Reynolds number. Most notably, the experiment is three-dimensional while the simulations shown here are two-dimensional. The experiment uses an airfoil while the simulations use a semi-infinite parabola to mimic the leading-edge region of the airfoil. In addition, the simulations contain no free stream perturbations (turbulence, acoustic, etc.), which are always present at some level during an experimental investigation (instead relying on impulsively started vortex shedding).

To help visualize the two flow regimes, two points (see Figure 3) have been selected. Point A corresponds to steady laminar flow while point B is a typical unsteady vortex shedding. Figure 4a shows the streamfunction contours of flow past the isolated roughness element at a roughness Reynolds number of $Re_k = 871$. As the figure shows, this flow is steady and produces a laminar separation bubble in two dimensions, which extends

far downstream from the roughness, as was mentioned in Section 2.2. These long separation regions will lead to large amplification of the T-S waves. Increasing the Re_k value to 958 produces fully unsteady flow with vortex shedding, as shown in Figure 4b. For clarity, the flow directly behind the roughness is displayed with streamfunction contours and the flow further downstream of the roughness uses vorticity contours to visualize the flow; both figures are snapshots in time.

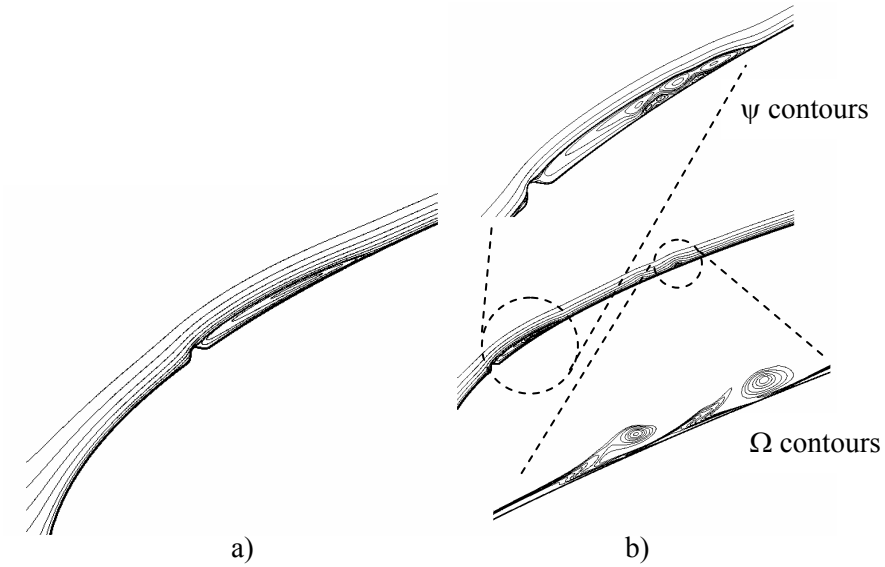

Figure 4. Laminar separation and unsteady vortex separation behind a single roughness element; a) Re_k=871, b) Re_k=958.

3.2 Three-dimensional Simulations

The three-dimensional Navier-Stokes code was validated for the case of steady flow over roughness by comparing with the numerical results of Davis *et al*. (1989). Figure 5 shows the streamwise skin friction on the roughness center-line. The flow over the roughness was computed for the same roughness element placed on parabolas of varying thickness. The third case, with R=0.01 reproduces the Davis *et al*. (1989) results for roughness on a flat plate. It should be noted that the local clean surface skin friction at the roughness location is the same for all three values of R, so that with the exception of the pressure gradient, flow conditions are approximately the same for each case. Bearing this in mind, Figure 5 reveals the first difference between roughness on a flat plate (R=0.01) and roughness on the airfoil leading edge (R=1). While the R=0.01 case is just separated behind the roughness, the R=1 case remains fully attached. Once the flow over the leading edge roughness separates, and as the roughness height continues to increase, the shear topology undergoes significant change.

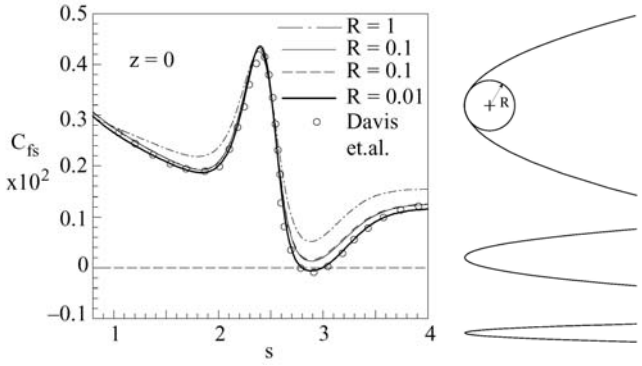

Figure 5. Comparison of the streamwise skin friction with Davis *et al*. (1989) for decreasing parabola thickness.

This shear topological change is shown in Figure 6 for increasing roughness height. Figure 6 shows that as the roughness height is increased, the shear topology features in the separation region downstream of the roughness change both in number and type.

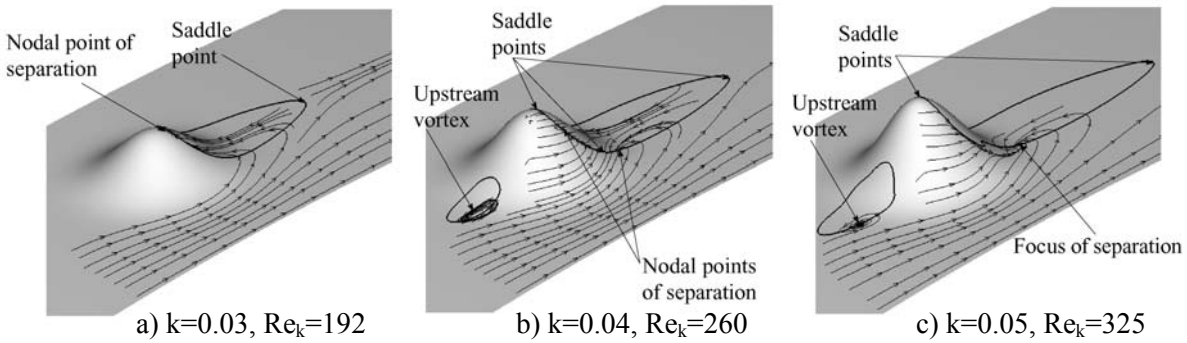

a) k=0.03, Re_k=192 b) k=0.04, Re_k=260 c) k=0.05, Re_k=325

Figure 6. Shear topological change for increasing roughness height.

Parameter studies show that this change in the shear topological structure is primarily a function of Re_k for a fixed roughness shape. The final case, Figure 6c, shows saddle points at separation and re-attachment and a focus of separation where a vortex is leaving the surface. This is the surface signature of the chimney vortices observed by Gregory & Walker (1956). Inserting stream-tracers into the flow near the location of the foci of separation reveals these chimney vortices in the Navier-Stokes calculations of Figure 7a, which is the same calculation as Figure 6c.

Figure 7b is a sketch of the vortex structures generated by a three-dimensional roughness element, from Gregory and Walker (1956), and is based on experimental observation. Examining Figure 7b, once the chimney vortices reach the roughness height they are turned downstream where they form a pair of counter-rotating streamwise vortices, also shown in the Gregory & Walker (1956) sketch. The downstream vertical plane in Figure 7a shows streamwise vorticity contours. The nearly circular contours indicate the presence of the streamwise vortices emanating from the chimney vortices while the more elliptical contours are evidence of the trailing legs of a horseshoe vortex, also depicted in the Gregory & Walker (1956) sketch, Figure 7b. The vortex structures may be significant in the future development of linear stability theories. With the

streamwise vorticity included as part of the base flow, Morkovin (1984) notes that the resulting primary instability will now contain a powerful vorticity-generating mechanism which is absent in instability theories for planar flows.

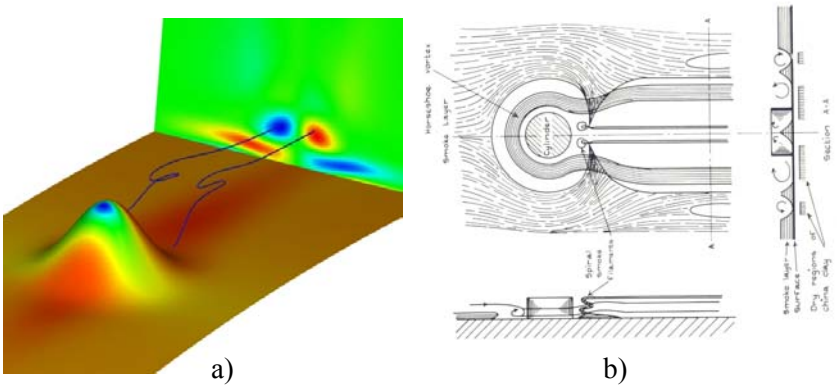

a) b)

Figure 7. Vortex structures in the wake of an isolated three-dimensional roughness. Qualitative comparison with Gregory & Walker (1956).

As mentioned previously, when Re_k is increased a value is reached at which the shear layer downstream of the roughness becomes unstable and hairpin vortices are shed periodically into the wake. These hairpin vortices may play a role in the onset of transition due to isolated three-dimensional roughness. Figure 8a shows the legs of the hairpin vortices which are shed into the wake at an Re_k of 750. The legs are depicted by displaying iso-surfaces of instantaneous streamwise vorticity. By comparison, Figure 8b is a sketch of hairpin vortex formation based on the experimental observations of Acarlar & Smith (1987) at the same value of Re_k. It should be noted that due to limited computational resources the DNS calculation has only been checked for grid independence in two dimensions. The spanwise grid spacing is approximately the same as the streamwise grid spacing. Future work will establish grid independence in three dimensions as well.

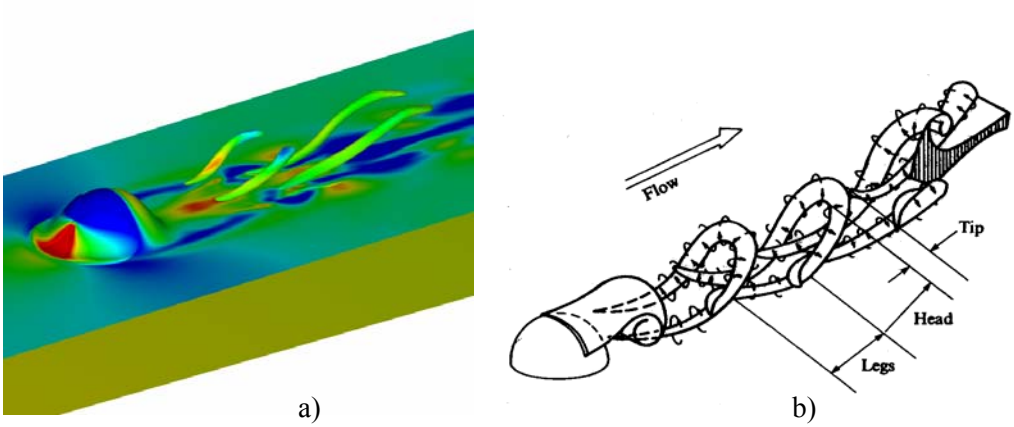

a) b)

Figure 8. a) Hairpin vortex legs illustrated with streamwise vorticity iso-surfaces, from DNS calculations. b) Hairpin vortex shedding sketch based on the experimental observations of Acarlar & Smith (1987).

At much higher values of Re_k, the vortex shedding is much less regular. Figure 9 shows two wall normal velocity iso-surfaces resulting from a DNS computation of the Winkler (1996) isolated roughness experiment. The Re_k of the computation and experiment is 3700. Upstream of the roughness there is evidence of the horseshoe vortex structure. Just downstream of the roughness there appears to be a vortex shedding which is periodic but not nearly as regular as that shown in Figure 8a.

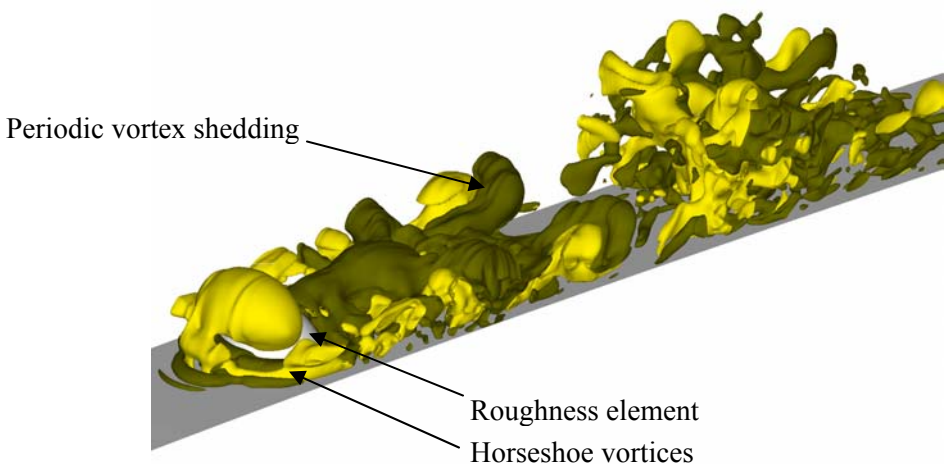

Figure 9. Instantaneous wall-normal velocity iso-surfaces (yellow=positive,upward, green=negative,downward)

It should be noted that because of the high value of Rek used in the computation grid independence could not be established in the wake region despite using 0.25 million grid points per roughness height length in the streamwise direction. However, grid independence was achieved upstream of the roughness. Figure 10 shows a comparison of the time-averaged wall normal velocity contours between the Winkler (1996) data and the computational results.

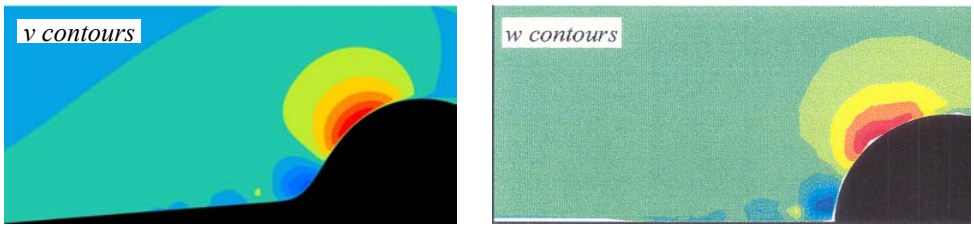

a) b)

Figure 10. Comparison of time-mean wall-normal velocities between Winkler (1996) experiment and DNS results.

The favourable comparison in the upstream region shows the ability of the DNS code to predict the vortex structures in this region (i.e. the time-averaged horseshoe vortices). Similar results have been seen for time-averaged streamwise velocity contours.

Because of the high computational cost of DNS the question often raised is whether “real life” flows can be simulated. In most cases they cannot, however, the information that is of interest can often be extracted from

lower Reynolds number simulations of flow over the same geometry. The key is running the simulation at a Reynolds number which gives an appreciable separation between the scales at which the turbulent energy is produced and the scales at which the energy is dissipated, Moin & Mahesh (1998). Figure 11 shows a comparison between computation and experiment where the computation is run at a much lower Reynolds number. Both parts of the figure show time averaged streamlines. Note that the time-averaged vortex structure upstream of the roughness is similar in both cases. Downstream there is also a qualitative similarity in the vortex structure. The difference is the stand-off distance of the vortex head from the roughness in the lower Reynolds number case.

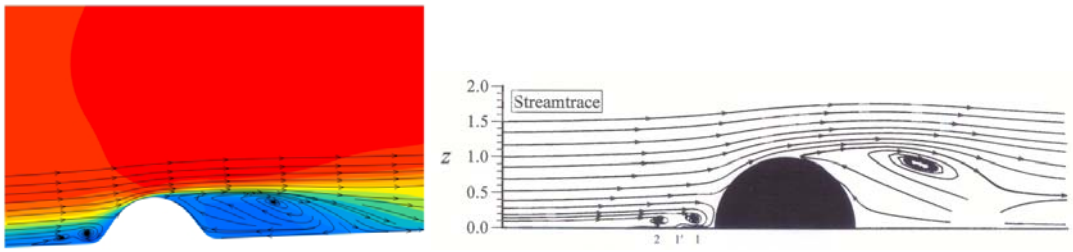

a) b)

Figure 11. a) Time-averaged streamwise velocity contours and time-averaged streamlines from a simulation with Re_k=750. b) Time-averaged streamlines from Winkler (1996) experiment with Re_k=3700.

It should again be noted that grid independence has not yet been verified in three-dimensions for the computation of Figure 11a.

4.0 SIMULATION OF SURFACE ROUGHNESS DISTRIBUTIONS

4.1 Two-dimensional Simulations

One of the primary comparisons for the two-dimensional Navier-Stokes with distributed leading-edge roughness was with the experimental work by Bragg *et al.* (1995). The experimental distributed roughness consisted of hemispheres placed in staggered rows with a height of 0.35mm. For comparison, the 1/4" roughness case was selected, which refers to the chordwise extent of the roughness field. The start of the roughness field is at a surface arc length of 7mm from the leading edge, while the aft edge of the roughness is at a surface arc length of 13.25mm. The spacing of the roughness elements (center-to-center) is 1.3mm. It should be noted that the work by Bragg *et al.* (1995) uses three-dimensional hemispheres, whereas the computations discussed in this section use two-dimensional quartic roughness elements. The reference airfoil used in the experimental work is a NACA 0012 with a chord length of 21".

Bragg *et al.* (1995) used three different chord Reynolds numbers in their study. In the two-dimensional simulations, comparisons are made with the first two values: $Re_c = 0.75 \times 10^6$ and $Re_c = 1.25 \times 10^6$. At the lower Reynolds number, the flow in the roughness region is steady, laminar flow. When the chord Reynolds number is increased, the flow becomes fully unsteady, with vortex shedding. Figure 12 shows a picture of the vortex shedding simulations downstream of the two-dimensional distributed roughness obtained by plotting the vorticity contours for the $Re_c = 1.25 \times 10^6$ case. Fasel, *et al.* (1976) postulates that surface roughness producing this type of vortex shedding acts as a source of additional disturbances and augments the inherent natural disturbances which occur, and this can promote early transition.

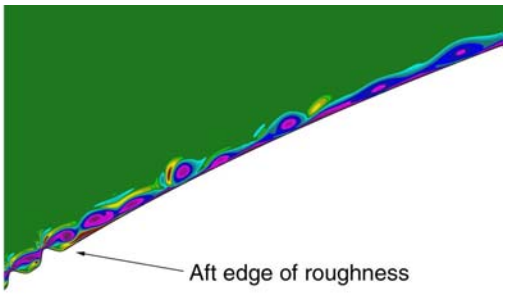

Figure 12. Vorticity contours showing the vortex shedding downstream of two-dimensional distributed roughness for a chord Reynolds number of $Re_c = 1.25x10^6$.

The experimental work also provided turbulence intensity profiles for various chord locations downstream of the distributed roughness. Figure 13 shows the experimental results for the NACA 0012 with the 1/4" roughness at $Re_c = 1.25x10^6$ for x/c = 0.05. The plot also includes the "fluctuation intensity" profile for the corresponding location on the parabola leading edge. The turbulence intensity is defined to be the root-mean square of the perturbation velocity. The algorithm uses the same equation as the experimental turbulence intensity (but in two-dimensions) to generate the fluctuation intensity values. This plot shows that the overall magnitude and trends of the two-dimensional Navier-Stokes results are in fair agreement with the experimental results. Any discrepancies could be caused by three-dimensional effects. The results of two different grids, 1501x201 and 1101x101, are also provided, which show good grid refinement of the time-averaged profiles.

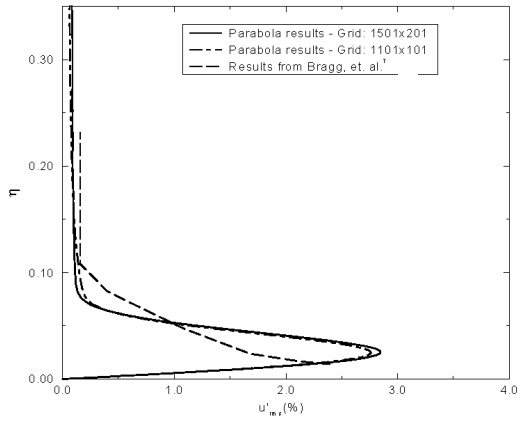

Figure 13. A comparison of fluctuation intensity profiles to a turbulence intensity profile from the experimental work of Bragg, *et al*. (1995) for the 1/4" roughness at x/c = 0.05.

4.2 Three-dimensional Simulations

The three-dimensional version of the DNS code has also been used to compute the lower Reynolds number case of Bragg *et al*. (1995) for flow over the three-dimensional distributed roughness field on an airfoil leading edge. Although the case shown here ($Re_c = 0.75x10^6$) does not induce early transition, the computational results are useful for examining the vortex structures which may play a role in the transition

process at slightly higher Reynolds numbers. Figure 14 shows the spanwise vorticity on the roughness surface as well as the streamwise vorticity on the downstream plane.

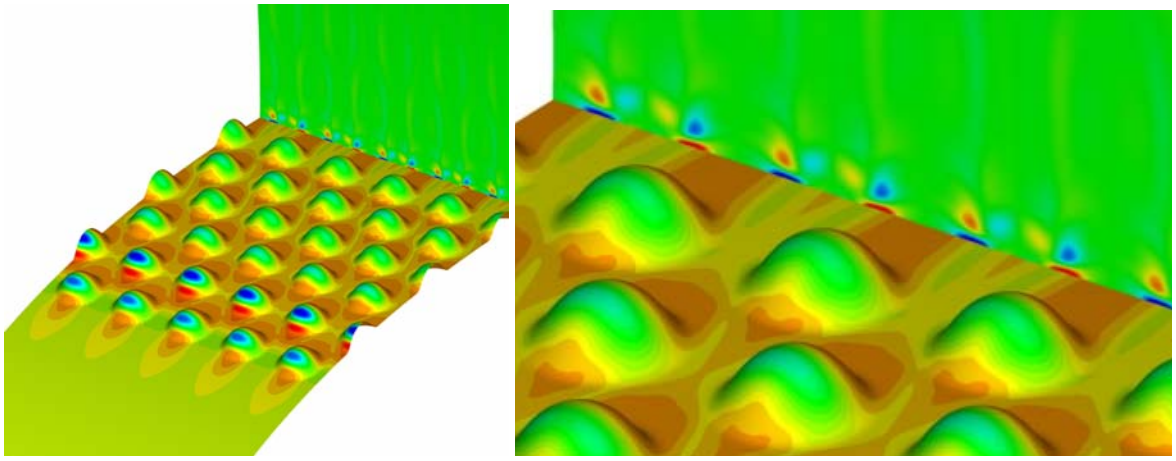

a) b)

Figure 14. Spanwise (roughness surface) and streamwise (downstream plane) vorticity over a roughness field

The flow over the first two rows of roughness elements is accelerated over the top of the roughness, as indicated by the dark blue regions near the roughness peaks. The downstream elements, which appear to be in the shadow of the front two rows, do not experience nearly the same acceleration. Additionally, the streamwise vorticity pattern on the downstream plane (shown in Figure 14b) is somewhat more complex than for the isolated roughness (Figure 7a). For an isolated hemispherical roughness the downstream counter-rotating streamwise vortices (i.e. trailing vortices) are spaced approximately one roughness diameter apart. For the roughness pattern shown in Figure 14, the trailing vortices which are generated by the second-to-last row of elements are "pinched" by downstream elements. Additionally, these trailing vortices are located very near to the trailing vortices which are generated by the downstream elements.

5.0 CONTROL OF LEADING EDGE SEPARATION WITH DYNAMIC ROUGHNESS

This section focuses on the investigation of the effects of dynamic roughness on the local flow physics. Currently, only two-dimensional simulations have been performed with the dynamic roughness. With respect to implementing dynamic roughness as a flow control mechanism, two primary cases are investigated: 1) flow separation at a constant angle-of-attack and 2) flow separation due to dynamic stall. As expected, the full dynamic roughness configuration which can impact flow separation is different for constant angle-of-attack and for dynamic stall, and includes such factors as roughness location and maximum height. It should be noted that for both the constant angle-of-attack and dynamic stall cases, effort was made to find a combination of parameters which produced a positive impact on flow separation. However, no effort has been made to optimize these parameters for a given flow condition.

For the static case, the angle-of-attack was chosen such that an unsteady flow separation is produced on the upper surface of the clean leading edge at a given Reynolds number. The angle-of-attack parameter is set at

K(t) = 2.0 and the Reynolds number based on leading-edge radius is 1000. Using a NACA 0012 airfoil for reference, these values correspond to an angle of attack of 21 degrees and a chord Reynolds number of 0.7×10^5. Three separate cases are investigated, which all have the same angle of attack and the same freestream Reynolds number: 1) clean airfoil with no roughness, 2) static roughness set to match the maximum expansion of the dynamic roughness, and 3) dynamic roughness. Figure 15a shows streamfunction contours for the clean airfoil with an unsteady flow, a leading-edge recirculating region and small vortices being shed downstream of the unsteady reattachment. The static roughness case is shown in Figure 15b. This streamfunction plot is made at the same time as the solution for the clean airfoil. The static roughness clearly shows the formation of a primary vortex and a secondary vortex, along with a shed vortex which is being convected downstream. The flow separation is similar to the clean surface, but with more unsteadiness for the case with the surface roughness. The static roughness height is approximately 70% of the oncoming boundary layer height.

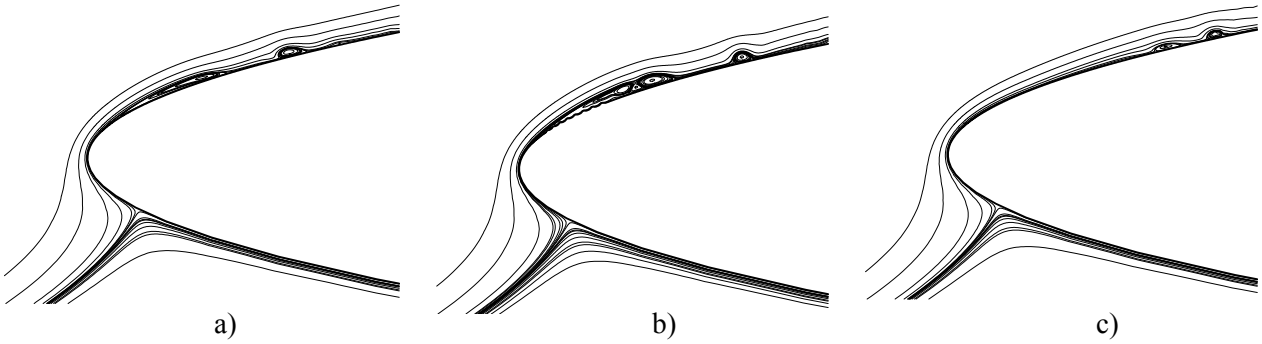

Figure 15. Leading-edge flow separation at a static angle-of-attack (showing streamfunction contours) for: a) clean airfoil, b) airfoil with static roughness, c) airfoil with dynamic roughness (fully contracted at physical time.

The last case (Figure 15c) uses the dynamic roughness in place of static roughness. As the dynamic roughness expands in time, the maximum height matches the static roughness height. For this flow separation case, the dynamic roughness produces a significantly different flow pattern at this angle-of-attack. The primary and secondary vortices formed in the leading-edge region are non-existent with dynamic roughness present. Only small downstream vortices are seen in the streamfunction plot of Figure 15c. The dynamic roughness suppresses the main leading-edge flow separation. It was found during testing that if the maximum dynamic roughness height exceeded the boundary layer height, the dynamic motion became detrimental to flow control and the severity of the flow separation increased. Therefore, the size of the dynamic roughness perturbations is a crucial element in the application of flow control. Folk & Ho (2001) came to the same conclusion, that the relative size of the perturbation with respect to the boundary layer height is a key factor in determining what effect the moving boundary has on the flow. The roughness is located in the vicinity of first separation on the clean airfoil surface. Several locations of dynamic roughness were attempted for this flow simulation, which resulted in negligible impact; some of the locations and maximum roughness heights produced results similar to the static roughness case. A preliminary conclusion is that each individual flow condition will require a slightly different dynamic roughness configuration. In addition, the dynamic roughness must be located near the separation point, which is also noted by Folk & Ho (2001) and Gad-el-Hak (2001). It is also assumed that for optimal flow control the required frequency of the dynamic roughness will be dependent on the freestream conditions. The current preliminary results only use one frequency for the dynamic roughness, which oscillates at a frequency of approximately 60 Hz.

The second flow separation case investigated is dynamic stall; the airfoil leading edge is pitched up at a rapid rate to promote the formation of the dynamic stall vortex. Huebsch & Rothmayer (2002) have shown that dynamic stall is a robust process that is typically unaltered by small levels of static surface perturbations. The same three surface configurations used in the constant angle-of-attack case are used for the dynamic stall, along with the same Reynolds number. As with the previous case, a laborious search through parameter space was required to find a dynamic roughness configuration that could impact the dynamic stall. The same basic roughness geometry used for the constant angle-of-attack case is also used here. However, the chord location and maximum roughness height were altered for the dynamic stall case. Most combinations that were attempted had no effect on the formation of the dynamic stall vortex.

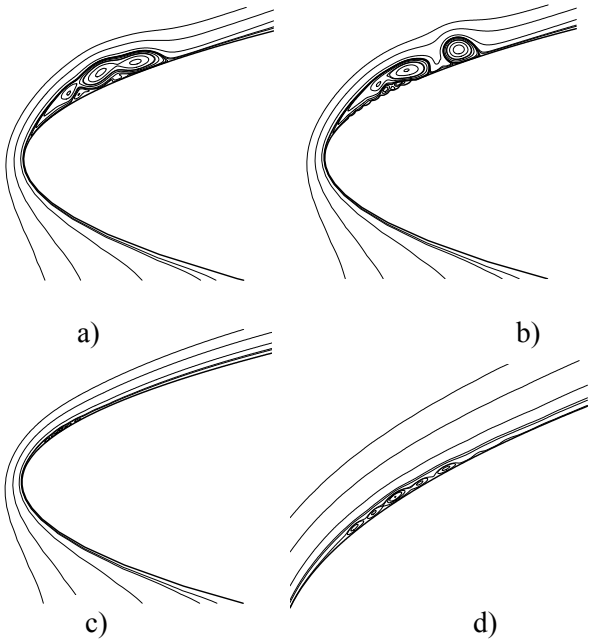

Figure 16. Leading-edge flow separation with dynamic stall conditions (t = 35) (showing streamfunction contours) for: a) clean airfoil, b) static roughness, c) dynamic roughness, and d) dynamic roughness with enhanced local view.

Figure 16a shows the clean airfoil undergoing the dynamic stall maneuver at non-dimensional physical time of t = 35. The dynamic stall vortex is fully formed at this point with primary, secondary, and tertiary vortices visible in the leading-edge region. This temporal station of the unsteady vortex formation is just prior to a primary vortex being shed from the surface and convected downstream. The result of adding static surface roughness is shown in Figure 16b, which is the same airfoil as Figure 16a at the same physical time. The formation of the dynamic stall vortex is similar to the clean case, but the static roughness has slightly hastened the process; a primary vortex has already been shed from the surface and is being convected downstream. For much of the rapid pitchup process, the clean surface and static roughness results are quite similar. At later times, the surface roughness accelerates the unsteady vortex formation. The final surface configuration uses dynamic roughness on the leading edge, as shown in Figure 16c. The dynamic roughness is able to suppress the initial formation of the dynamic stall vortex. This is a significant result given the fact that the dynamic stall process is fairly robust. The streamlines are shown at the same physical time as the previous figures in the pitchup sequence and, as noted, the dynamic roughness is in the fully contracted position in this snap-shot.

Zooming into the region on the upper surface where the dynamic roughness is located (Figure 16d), one can see small unsteady eddies being formed, though they are smaller than the local boundary layer height. These small eddies are present throughout much of the pitchup sequence, but remain localized within the boundary layer. Typically the first phase of the dynamic stall process is the formation of a long separation region on the upper surface of the leading edge. At t = 35 with the dynamic roughness, this bubble has not yet formed. At t = 39, the first primary vortex is just starting to form on the leading edge. Therefore, the dynamic roughness has the ability to significantly delay the formation of the dynamic stall vortex and allow the airfoil to reach a higher angle of attack, hence a higher maximum lift coefficient, for the flow conditions tested in this study.

6.0 CONCLUSION

When natural surface roughness exists on an airfoil leading edge it can have a detrimental impact on the airfoil performance. Key to this performance loss is the premature transition which is initiated by the roughness. For two-dimensional and isolated three-dimensional roughness, the transition process is related to the separation and vortex structures generated by the roughness. It is likely that these structures also play an important role in distributed roughness induced transition. For this reason, characterization of the separation and vortex structures generated by leading edge roughness is an important step towards understanding the effect of roughness on airfoil performance. This paper has outlined a DNS approach which is able to address this issue. Preliminary validation of the code has been made with experimental results. The calculations have shown the ability of the DNS approach to capture the critical long separation regions downstream of two-dimensional roughness as well as horseshoe, chimney and hairpin vortex formation in the wake of isolated three-dimensional roughness, and streamwise vortex pairs generated by distributed roughness fields.

In addition, preliminary two-dimensional computations suggest that synthetic surface roughness has the potential to be used as a means of flow control by delaying separation under certain conditions. This paper has shown that the DNS approach is able to analyze those situations in which dynamic roughness may suppress leading edge separation at large angle-of-attack or rapid pitchup. In both cases the dynamic roughness was shown to delay the formation of the separation bubble, and may lead to an increase in the airfoil performance.

7.0 REFERENCES

[1] Acarlar, M.S., & Smith, C.R., “A study of hairpin vortices in a laminar boundary layer,” *Journal of Fluid Mechanics*, Vol. 175, pp. 1-41, 1987.

[2] Aldoss, T.K., *Initial value study of effect of distributed roughness on boundary layer transition,* Ph.D. Thesis, Case Western Reserve University, 1982.

[3] Boer, J.N., & Van Hengst, J., “Aerodynamic degradation due to distributed roughness on high lift configuration,” AIAA paper 93-0028, presented at the 31st Aerospace Sciences Meeting & Exhibit, 1993.

[4] Bragg, M.B., & Gregorek, G.M., “Environmentally induced surface roughness effects on laminar flow airfoils: Implications for flight safety,” AIAA paper 89-2049, presented at the Aircraft Design, Systems, and Operations conference, 1989.

[5] Bragg, M.B., Kerho, M.F. & Cummings, S.L., "Airfoil boundary layer due to large leading-edge roughness," AIAA paper 95-0536, presented at the 33rd Aerospace Sciences Meeting & Exhibit, 1995.

[6] Bragg, M.B., Cummings, S.L., & Henze, C.M., "Boundary-layer and heat transfer measurements on an airfoil with simulated ice roughness," AIAA paper 96-0866, presented at the 34th Aerospace Sciences Meeting & Exhibit, 1996.

[7] Braslow, A.L., Hicks, R.M., & Harris, R.V., "Use of grit-type boundary-layer transition trips on wind-tunnel models," NASA TN D-3579, Sept. 1966.

[8] Brumby, R.E., "Wing surface roughness, cause and effect," *DC Flight Approach*, Jan. 1979.

[9] Bushnell, D.M., Hefner, J.N., and Ash, R.L., "Effect of Compliant Wall Motion on Turbulent Boundary Layers," *Physics of Fluids*, Vol. 20, Pt. II, pp. S31-S48, 1977.

[10] Bushnell, D.M., "Notes on initial disturbance fields for the transition problem," NASP Technical Memorandum 1051, March, 1989.

[11] Cebecci, T., & Egan, D.A., "Prediction of transition due to isolated roughness," *AIAA Journal*, Vol. 27, 1989.

[12] Corke, T.C., Bar-Sever, A., & Morkovin, M.V., "Experiments on transition enhancement by distributed roughness," *Physics of Fluids*, Vol. 29, No.10, pp. 3199-3213, 1986.

[13] Cummings, M.J., and Bragg, M.B., "Boundary-layer transition due to isolated three-dimensional roughness on airfoil leading edge," Technical Note, *AIAA Journal*, Vol. 34, No. 9, pp. 1949-1952, 1996.

[14] Davis, R.L., Carter, J.E, & Hafez, M., "Three-dimensional viscous flow solutions with a vorticity-stream function formulation," *AIAA Journal*, Vol. 27, pp. 892-900, 1989.

[15] Duck, P.W., "Laminar Flow Over Unsteady Humps: The Formation of Waves," *J. Fluid Mechanics*, Vol. 160, pp. 465-498, 1985.

[16] Duck, P.W., "Triple-Deck Flow Over Unsteady Surface Disturbances: The Three-Dimensional Development of Tollmien-Schlichting Waves," *Computers & Fluids*, Vol. 18(1), pp. 1-34, 1990.

[17] Fasel H., "Investigation of the Stability of Boundary Layers by a Finite-Difference Model of the Navier-Stokes Equations," *J. Fluid Mechanics*., Vol. 78(2), pp. 355-383, 1976.

[18] Fasel, H., Bestek, H., & Schefenacker, R., "Numerical simulation studies of transition phenomena in incompressible, two-dimensional flows," In: *Proceedings of the AGARD Symposium on Laminar-Turbulent Transition*, Copenhagen, 1977.

[19] Floryan, J.M., Yamamoto, K., & Murase, T., "Laminar-turbulent transition in the presence of simulated wall roughness," *Canadian Aeronautics and Space Journal*, Vol. 38, No. 4, pp. 173-182, 1992.

[20] Folk, C. and Ho, C.M., "Micro-Actuators for Control of Delta Wing with Sharp Leading Edge," AIAA Paper No. 2001-0121, 2001.

[21] Gad-el-Hak, M., "Flow Control: The Future," *AIAA Journal of Aircraft*, Vol. 38(3), pp. 402-417, 2001.

[22] Greenblatt, D. and Wygnanski, I.J., "The Control of Flow Separation by Periodic Excitation," *Progress in Aerospace Sciences*, Vol. 36, pp. 487-545, 2000.

[23] Greenblatt, D. and Wygnanski, I. J., "Dynamic Stall Control by Periodic Excitation, Part 1: NACA 0015 Parametric Study," *Journal of Aircraft*, Vol. 38(3), pp. 430-438, 2001a.

[24] Greenblatt, D. and Wygnanski, I. J., "Dynamic Stall Control by Periodic Excitation, Part 2: Mechanisms," *Journal of Aircraft*, Vol. 38(3), pp. 438-447, 2001b.

[25] Gregory, N., & Walker, W.S., "The effects of transition of isolated surface excrescences in the boundary layer," British ARC, Res. Memo. 2779, 1956.

[26] Hood, M.J., "The effects of surface waviness and of rib stitching on wing drag," NACA Technical Note No. 724, August, 1939.

[27] Huebsch, W.W., *Numerical investigation on the interaction between surface roughness and viscous flows*, Ph.D. Thesis, Iowa State University, 2000.

[28] Huebsch, W.W., & Rothmayer, A.P., "Unsteady Navier-Stokes simulation of flow past surface ice geometries," AIAA paper 2000-0232, presented at the 38th Aerospace Sciences Meeting & Exhibit, 2000.

[29] Huebsch, W.W., & Rothmayer, A.P., "Effects of surface ice roughness on dynamic stall," *Journal of Aircraft*, Vol. 39, No. 6, pp. 945-953, 2002.

[30] Huebsch, W.W., "Dynamic surface roughness for aerodynamic flow control," AIAA paper 2004-****, presented at the 42nd Aerospace Sciences Meeting & Exhibit, 2004.

[31] Huebsch, W.W., & Rothmayer, A.P., "Numerical prediction of unsteady vortex shedding for large leading-edge roughness," *Computers and Fluids*, Vol. 33, No.3, pp. 405-434, 2004.

[32] Kendall, J.M., "The effect of small-scale roughness on the mean flow profile of a laminar boundary layer," *Instability and Transition*, Vol. 1, Springer-Verlag, New York, pp. 296-302, 1990.

[33] Kerho, M.F., *Effect of large distributed roughness near an airfoil leading edge on boundary-layer development and transition,* PhD Dissertation, University of Illinois Urbana-Champaign, Urbana, IL, 1995.

[34] Kerho, M.F. & Bragg, M.B., "Airfoil boundary-layer development and transition with large leading-edge roughness," *AIAA Journal*, Vol. 35, No. 1, pp. 75-84, 1997.

[35] Klebanoff, P.S. & Tidstrom, K.D., "Mechanism by which a two-dimensional roughness element induces boundary-layer transition," *Physics of Fluids*, Vol. 15, pp. 1173-1188, 1972.

[36] Lekoudis, S.G. and Sengupta, T.K., "Two-Dimensional Turbulent Boundary Layers Over Rigid and Moving Swept Wavy Surfaces," *Physics of Fluids*, Vol. 4(29), pp. 965-970, 1986.

[37] Leventhal, L., *Preliminary experimental study of disturbances in a laminar boundary-layer due to distributed surface roughness,* MS Thesis, Case Western University, Cleveland, OH, 1981.

[38] Ljungstromm, B., "Wind tunnel investigation of simulated hoar frost on a 2-dimensional wing section with and without high lift devices," Report FFA AU-902, The Aeronautica Research Institute of Sweden, April, 1972.

[39] Masad, J.A., & Iyer, V., "Transition prediction and control in subsonic flow over a hump," *Physics of Fluids*, Vol. 6, No. 1, pp. 313-327, 1994.

[40] Matheis, B.D., Rothmayer, A.P., & Huebsch, W.W., "Three-dimensional steady Navier-Stokes calculations of flow past airfoil leading edge surface roughness," AIAA paper 2003-3725, presented at the 33rd Fluid Dynamics Conference & Exhibit, 2003.

[41] Matheis, B.D., & Rothmayer, A.P., "Impact of surface roughness on local aerodynamics using a three-dimensional Navier-Stokes solver," AIAA paper 2004-0058, presented at the 42nd Aerospace Sciences Meeting & Exhibit, 2004.

[42] Moin, P., & Mahesh, K., "Direct Numerical Simulation: A tool in turbulence research," *Annual Review of Fluid Mechanics*, Vol 30, pp. 539-578, 1998.

[43] Morkovin, M.V., "Critical evaluation of transition from laminar to turbulent shear layers with emphasis on hypersonically traveling bodies," AFFDL TR-68-149, 1969.

[44] Morkovin, M.V., "Bypass transition to turbulence and research desiderata," NASA CP-2386, pp. 161-204, 1984.

[45] Morkovin, M.V., "On roughness-induced transition: Facts, views and speculations," *Instability and Transition, Volume 1*, edited by M.Y. Hussaini and R.G. Voigt, Springer-Verlag, pp. 281-295, 1990.

[46] Morkovin, M.V., Reshotko, E., & Herbert, T., "Transition in open flow systems – A reassessment," *Bull. Am. Phys. Soc.*, Vol. 39, pp. 1882, 1994.

[47] Norman, R.S., *On obstacle generated secondary flows in laminar boundary-layers and transition to turbulence,* Ph.D. Thesis, Illinois Institute of Technology, 1972.

[48] Oolbekkink, B., & Volkers, D.F., "Aerodynamic effects of distributed roughness on a NACA 63_2-015 airfoil," AIAA paper 91-0443, presented at the 29th Aerospace Sciences Meeting & Exhibit, 1991.

[49] Peterson, J.B., & Horton, E.A., "An investigation of the effect of a highly favorable pressure gradient on boundary-layer transition as caused by various type of roughness on a 10-foot diameter hemisphere at subsonic speeds," NASA Memo 2-8-59-L, April 1959.

[50] Rediniotis, O., Lagoudas, D., Mani, R., Traub, L., Allen, R., and Karniadakis, G., "Computational and Experimental Studies of an Active Skin for Turbulent Drag Reduction," AIAA-2002-2380, 1st Flow Control Conference, St. Louis, MO, July, 2002.

[51] Saric, W.S., Reed, H.L., & White, E.B., "Stability and transition of three-dimensional boundary layers," *Annual Review of Fluid Mechanics*, Vol 35, pp. 413-440, 2003.

[52] Schlichting, H. & Gersten, K., *Boundary layer theory*, 8th Revised and Enlarged Edition, Springer-Verlag, Berlin Heidelberg, 2000.

[53] Seifert, A., Bachar, T., Koss, D., Shepshelovich, M, and Wygnanski, I., "Oscillatory blowing: a tool to delay boundary-layer separation," *AIAA Journal*, Vol. 31(11), pp. 2052-2060, 1993.

[54] Singh, K., & Lumley, J.L., "Effect of roughness on the velocity profile of a laminar boundary layer," *Applied Scientific Research*, Vol. 24, pp. 168-186, 1971.

[55] Sundaram, S., Viswanath, P.R., and Rudrakumar, S., "Viscous Drag Reduction Using Riblets on NACA 0012 Airfoil to Moderate Incidence," *AIAA Journal*, Vol. 34(4), pp. 676-682, 1996.

[56] Tadjfar, M., Reshotko, E., Dybbs, A., & Edwards, R.V., "Velocity measurements within boundary layer roughness using index matching," FED Publication 33, ASME, 1985.

[57] Tani, I., "Effect of two-dimensional and isolated roughness on laminar flow," *Boundary Layer and Flow Control*, edited by G.V. Lachmann, Vol. 2, Pergamon, Oxford, England, UK, pp. 637-656, 1961.

[58] Tani, I., Komoda, H., and Konatsu, Y., "Boundary-layer transition by isolated roughness," Report 375, Aeronautical Research Institute, University of Tokyo, Japan, Nov. 1962.

[59] Tani, I., "Boundary-layer transition," *Annual Review of Fluid Mechanics*, Vol. 1, pp. 169-196, 1969.

[60] Tezok, F., Kafyeke, F., & Cebeci, T., "Prediction of airfoil performance with leading edge roughness," AIAA paper 98-5544, presented at the 36th Aerospace Sciences Meeting & Exhibit, 1998.

[61] Valarezo, W.O., Lynch, F.T., & McGhee, R.J., "Aerodynamic performance effects due to small leading edge ice (roughness) on wings and tails," *AIAA Journal of Aircraft*, Vol. 30, No. 6, Nov.-Dec. 1993.

[62] Werle, M.J., & Davis, R.T., "Incompressible laminar boundary layers on a parabola at angle of attack: A study of the separation point," *Trans. ASME*, Paper No. 71-APM-31, 1971.

[63] White, E.B., & Saric, W.S., "Application of variable leading-edge roughness for transition control on swept wings," AIAA paper 2000-0283, presented at the 38th Aerospace Sciences Meeting & Exhibit, 2000.

[64] Winkler, J.F., *Local flowfield about large distributed roughness elements in a laminar boundary layer*, PhD Dissertation, University of Illinois at Urbana-Champaign, 1996.

AVT-111 Specialists' Meeting on Enhancement of NATO Military Flight Vehicle Performance by Management of Interacting Boundary Layer Transition and Separation

DISCUSSION

1. REFERENCE No. OF THE PAPER: 15
2. DISCUSSOR´S NAME: John Hourmouziadis
3. AUTHOR´S NAME: B.D. Mattheis

QUESTION:

The horse-shoe vortex is generated by the pressure rise along the stagnation streamline. Some of the simulations of experiments showed a filet radius at the leading edge at the roughness. This will reduce the intensity of the vortex and needs to be acknowledged if the horse-shoe vortex is of relevance to the object of the study.

AUTHOR´S REPLY:

Agreed. Though studying the horse-shoe vortex was not or primary importance in this study, comparison with experiment was good despite the filleted radius. It should be clarified that the simulation velocity profiles shown in the presentation and the paper shifted in the streamwise direction to account for the fact that the filleted geometry intersected the surface further upstream than the true hemisphere. This shift was applied consistently to all profiles with one roughness of the roughness. Outside of this region it was not necessary.